生体医工学
49(2)：387-389, 2011

創立50周年へのメッセージ

情報通信技術（ICT）は医療福祉問題の救世主か？

吉澤　誠*・杉田　典大**・阿部　誠**・西條　芳文***
本間　経康*・金野　敏†・山家　智之†・仁田　新一††

Is Information and Communication Technology (ICT) a Savior?

Makoto YOSHIZAWA,* Norihiro SUGITA,** Makoto ABE,** Yoshifumi SAIJO,***
Noriyasu HOMMA,* Satoshi KONNO,† Tomoyuki YAMBE,† Shin-ichi NITTA††

1. はじめに

数十年先の未来は予測しにくい．しかし，人口構成の推移だけは例外で，ほぼ確実な予測ができる．すなわち，少子高齢化が日本の医療における最大の課題であり，革命的な改革がなければ，医療保険制度ばかりでなく国の財政自体が確実に崩壊する．

すでにわが国では，医療サービスの地域格差が著しくなりつつある．特に過疎化が著しい東北地方では，多くの地方中核病院が医師不足によって存立の危機に陥っている．しかし，医師の絶対数を増やすことは医療費抑制に結びつかない．賢明な生体医工学会会員であれば先刻ご承知のように，問題の解決策のひとつとして有望なのは，医療サービスにおける情報通信技術（ICT）の活用である．

本稿では，医療におけるICTの応用に関する東北大学における取り組みを紹介するとともに，この分野における今後の生体医工学会への期待について述べる．

2. ICTは医療福祉問題の救世主か？

ICTは医療福祉問題の救世主のように思われている．しかし，インターネットやモバイル通信がこれほど普及しつつあるにもかかわらず，遠隔医療の進展速度は遅い．

著者は2001年のBMEに解説「IT革命が加速する人工臓器の計測・制御・通信の未来」[1]を著し，「今のところ，人工臓器のIT化を進めるための最もよい近道は，人工臓器より抵抗が少なく，超高齢化社会となって利用者の増大が予想される在宅医療のIT化と協力することである」と述べた．今から10年前のことである．そのころと比べて現在では民間の情報通信環境は格段の進歩を遂げている．モバイル通信のスピードは3GやWiMAXの登場で数十Mbps程度となり，携帯電話の多くはスマートフォンやタブレット型PCに移行しつつある．しかし，本格的な遠隔医療は未だ実現されていない．

過疎地域で病院に出向くことが困難な高齢者にはICTを使った遠隔医療が有用であることについては誰でも賛成するだろう．しかし今のところ，遠隔医療は特定の慢性疾患で再診のときに限り認められているに過ぎない．

遠隔医療の進展を促すには法律や制度の変更が必要である．それには医師や医療機関との調整，医療保険制度との整合性維持，介護分野との連携など，厄介な問題が山積している．また，ICTの導入が本当に医療福祉費の爆発の抑制に寄与するのかという問題がある．

これまで各省の補助金により各地で多くの遠隔医療実験が行われてきた．しかし，補助金が途絶えると消えてしまう事例が多かった．今のところ遠隔医療は儲からないし，遠隔医療に身銭を切る患者はあまり多くないからだろう．

3. 東北地方での取り組み

東北大学では，2003年4月から加齢医学研究所に臨床医工学寄附研究部門を設置し，遠隔医療を中心とした「IT外来構想」の実現に向けた研究に取り組んできた．さらに，東北大学，宮城県および仙台市は，2007年10月からICTに基づく先進予防型健康社会を目指した「広域仙台地域知的クラスター創成事業（第II期）」（2010年度か

* 東北大学サイバーサイエンスセンター先端情報技術研究部
** 東北大学大学院工学研究科
*** 東北大学大学院医工学研究科
† 東北大学加齢医学研究所
†† (社)医療福祉事業推進機構

ら諸事情により「地域イノベーションクラスター事業」[2]に名称変更）を展開している．

この一環として著者らは，2009年3月4日に関係企業とともに「モバイル環境における医療情報通信システム開発コンソーシアム」を設立し，高画質映像を中心とした生体情報を，携帯電話，PHS，WiMAXなどのモバイル通信系を利用することにより，いつでもどこでも簡便に伝送することのできる，**図1**および**図2**のような遠隔医療システム「電子診療鞄」の開発を開始した[3, 4]．

他の遠隔医療システムでは患者宅に医療端末を据え置くタイプが多いのに対して，電子診療鞄は訪問診療向けのシステムである．

2006年度の医療保険制度の改正により，24時間体制で往診や訪問看護を実施するための診療所を普及させるための仕組みとして「在宅療養支援診療所」制度が始まった．しかし，小規模の診療所の場合，医師が24時間365日の不眠不休の体制を強いられる可能性があるなど労働環境が苛酷であるばかりでなく，訪問看護ステーションとの連携などにかかるコストが大きい上，患者宅への移動時間が診療効率を落としている．

電子診療鞄は，このような状況を改善するためのもので

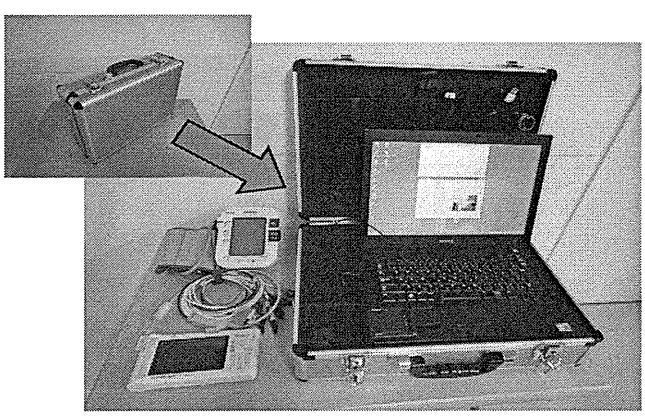

図1　電子診療鞄の外観[4]．

図2　電子診療鞄の実証実験[4]．

あり，これを持参した看護師が医師の代わりに患者宅を訪問し，病院や診療所にいる医師と在宅患者との間の等価的な対面診療環境を実現できる．

もし，すべての家庭で固定インターネット回線が使えるのであれば，既存のテレビ会議システムやSkypeなどの家庭向けテレビ電話システムに医療用データを伝送する機能を付加するだけで対面診療や遠隔見守りに近い環境が実現できる．据え置き型のヘルスケア装置はこのようなタイプのものである．

これに対して電子診療鞄では，モバイル通信環境を利用することで，固定インターネットが使えない独居高齢者宅や救急車などでも，ハイビジョン画質の超音波エコー像などに基づく遠隔医療を実現しようとするものである．患者自身や家族に医療機器を操作させることが法的にも技術的にも困難であり看護師が赴くことが前提であるのであれば，高価な機器を各家庭に据え置く必要はなく，本装置のような形態の方が普及しやすい可能性がある．

また，電子診療鞄では中央サーバを介したデータ伝送を行うため，一般のインターネット回線に接続された認証を受けたPCを利用することによりセキュアな形で複数の医師によるデータ共有が可能である．

すなわち，電子診療鞄を利用する対象は，訪問診療や在宅医療を行う診療所，これらと関係の深い地域連携病院，および訪問看護ステーションなどの医療事業者等であることが想定される．ただし，高速化が進みつつあるモバイル通信の利点を生かし，生体計測用端末装置の組み合わせを変更することにより，離島，僻地，集団健診，イベント会場，救急車，災害現場などに利用フィールドを拡げることが可能であると思われる．また，電子診療鞄は単独で利用するばかりでなく，患者データベース，医師間連携システム，電子カルテシステムと連携することでより効率的なシステムとなる可能性がある．

2009年からこれまで，著者らは宮城県内の複数の診療所と中核病院や沖縄県宮古島において電子診療鞄の実証実験を行ってきた．その結果，システム全体について医師・看護師の診断に関する評価は高いが，操作性のさらなる改善が必要であることが指摘された．また．患者がこのような電子機器による遠隔診断を受け入れてくれるかどうかについても危惧していたが，実際に不安感を抱いた患者はほとんどいなかった．これは，このシステムでは看護師が必ず付き添うからであると思われる．

電子診療鞄の大きな問題は通信環境が一定しないことである．すなわち，モバイル通信ネットワークのトラフィックが混んでデータ伝送に時間がかかると受信側で動画像の遅延やフリーズが生じる可能性がある．これは，使用している地域，時間帯，モバイル通信ネットワークの種類等に大きく依存しており，特に救急車などでの運用にあたっては事前の調査が必要である．また，ネットワークの混み具

合によって画質を動的に変化させたり，使用するキャリアを切り替えるなどの機能も必要であろう．

4. これからの生体医工学会に期待するもの

どの学会でも苦労しているのは若い学生を如何にして学会に引き付けるかということである．東北大学では2008年度に大学院医工学研究科が創設され，工学部情報知能システム総合学科にメディカルバイオエレクトロニクス・コースができて以来，「医工学をやりたい」と応募する学生が増えてきた．このような傾向が生体医工学会にも波及するとよいと思われる．しかし，出口の段階で彼らを受け入れてくれる医療関係企業が増えないと後々問題となる．

今後，ICTあるいは医工学自体が，本当に医療福祉問題の解決手段になって行けば，情報通信系を問わず工学系の学生や技術者が新たに生体医工学会に入会する可能性も高まるだろう．

しかしそのためには，生体医工学会や遠隔医療学会などが主体となり，遠隔医療などの医工学的な先端医療がごく普通の医療であると認められるように，政府省庁・医療関係者に働きかけていくことが望まれる．

5. おわりに

最近，携帯電話より一回り程度大きい超小型の超音波診断装置が発売され，開業医が往診の際によく使用しているという．確かに往診先で超音波診断ができることは画期的である．しかしそれ以上に，この装置を媒介として医師と患者との間の会話が増えたということが予想外の効果のようである．

上述した電子診療鞄は医師ではなく看護師が患者宅に持参し，診療所にいる医師との間で通信をするシステムである．しかし患者にとっては，生身の医師に往診に来てもらって直に会話できることが最もよい．

言うまでもなく，ICTは医療福祉にとって有効なものであるが万能ではない．医工学を志す者は心得ておくべきことと思う．

文　献

1. 吉澤誠, 田中明, 阿部健一, 竹田宏, 山家智之, 仁田新一: IT革命が加速する人工臓器の計測・制御・通信の未来. BME. **15**(4): 16-22, 2001.
2. http: //www. mext. go. jp/component/a_menu/science/micro_detail /__icsFiles/afieldfile/2010/10/07/1297967_8.pdf
3. Yoshizawa M, Yambe T, Konno S, Saijo Y, Sugita N, Sugai T K, Abe M, Sonobe T, Katahira Y, Nitta S: A mobile communications system for home-visit medical services: The Electronic Doctor's Bag. 32nd Annual International Conference of the IEEE Engineering in Medicine and Biology Society. (CD-ROM), Buenos Aires, Argentina, 2010.
4. 杉田典大, 吉澤誠, 山家智之, 西條芳文, 金野敏, 仁田新一: 電子診療鞄の展開と評価. 日本遠隔医療学会雑誌. **6**(2): 207-210, 2010.

吉澤　誠（ヨシザワ　マコト）

1978年東北大学大学院工学研究科博士後期課程修了．工学博士．東北大学工学部助手，助教授，豊橋技術科学大学工学部助教授，東北大学大学院情報科学研究科助教授を経て，2000年情報シナジーセンター教授．2008年サイバーサイエンスセンター教授．1999年米国ジョンズホプキンズ大学医学研究所および米国ベーラー医科大学医学部客員研究員．人工心臓の知的制御・監視，バーチャルリアリティの医療応用，映像の生体影響評価に関する研究などに従事．計測自動制御学会評議員，日本生体医工学会評議員，IEEE Engineering in Medicine and Biology Society理事．

NANO-BIOMEDICAL ENGINEERING 2012

Proceedings of the Tohoku University Global Centre of Excellence Programme

Global Nano-Biomedical Engineering Education and Research Network Centre

Sakura Hall, Tohoku University,
Sendai Japan, 5 – 6 March 2012

Editor

Takami Yamaguchi, MD PhD
School of Biomedical Engineering, Tohoku University

Published by

Imperial College Press
57 Shelton Street
Covent Garden
London WC2H 9HE

Distributed by

World Scientific Publishing Co. Pte. Ltd.
5 Toh Tuck Link, Singapore 596224
USA office: 27 Warren Street, Suite 401-402, Hackensack, NJ 07601
UK office: 57 Shelton Street, Covent Garden, London WC2H 9HE

British Library Cataloguing-in-Publication Data
A catalogue record for this book is available from the British Library.

NANO-BIOMEDICAL ENGINEERING 2012
Proceedings of the Tohoku University Global Centre of Excellence Programme

ISBN-13 978-1-84816-905-0
ISBN-10 1-84816-905-1

Printed in Singapore by Mainland Press Pte Ltd.

PREFACE

It is my great pleasure to publish this bound compilation of the achievements of our Tohoku University Global Centre of Excellence (GCOE) Programme from 2007 to 2011 titled "Global Nano-Biomedical Engineering Education and Research Network Centre". The programme was promoted by the Ministry of Education, Culture, Sports, Science, and Technology of Japan and succeeded the 21st Century COE Programme. We at Tohoku University were awarded consecutive 21st Century COE and GCOE programmes in biomedical engineering, and ours was the only programme in this field to be awarded both. Moreover, during the current GCOE programme, the Graduate School of Biomedical Engineering was inaugurated at Tohoku University based on these activities in 2009. The Graduate School of Biomedical Engineering is the first and only purpose-built independent graduate school for biomedical engineering in Japan. This book comprises the final reports of the GCOE programme, including contributions from faculty, post-doctoral fellows, and students.

When we started the GCOE programme in 2007, we declared that nanoscale biomedical engineering is undoubtedly the most rapidly growing field of engineering and will become the most important one because of the incredibly rapid developments in science and technology in this area, especially the biological sciences. With the accelerating growth of biological engineering studies, we believe that we have played a pivotal role with our cross-disciplinary studies involving engineering and biology. It would be our great pleasure if those who read this book can benefit from our multi- and inter-disciplinary studies.

Both Tohoku University and the city of Sendai were gravely damaged by the East Japan Earthquake of 11 March 2011. The engineering school campus, which is located atop hills west of the city, was partially destroyed. The Electronics and Communications, Material Sciences, and Civil Engineering Departments were seriously damaged, disrupting the biomedical engineering education and research activities conduced in those departments as part of our GCOE programme for several months. Nevertheless, we are delighted to announce that activities returned to almost normal by the end of the 2011 academic year, and we ultimately produced more excellent graduates that year.

When we were affected by the disaster, many friends and colleagues worldwide expressed their sympathy and took action to help us. We are

Nano-Biointervention

using photoplethysmography. In: *Nano-Biomedical Engineering 2009*, Imperial College Press, UK, 411–419 (2009).
4. J. Allen and A. Murray, Modelling the relationship between peripheral blood pressure and blood volume pulses using linear and neural network system identification techniques. *Physiological Measurement* **20**, 287–301 (1999).
5. X. F. Teng and Y. T. Zhang, An evaluation of a PTT-based method for noninvasive and cuffless estimation of arterial blood pressure. *Proceedings of the 28th IEEE EMBS Annual International Conference*, New York, 6049–6052 (2006).
6. J. Y. A. Foo, C. S. Lim and P. Wang, Evaluation of blood pressure changes using vascular transit time. *Physiological Measurement* **27**, 685–694 (2006).

DETECTION OF LIFE-THREATENING ARRHYTHMIAS USING MULTIPLE REGRESSION MODEL

MAKOTO ABE[1)*], TELMA KEIKO SUGAI[2)], MAKOTO YOSHIZAWA[3)†], KAZUO SHIMIZU[4)], MOE GOTO[4)], MASASHI INAGAKI[5)], MASARU SUGIMACHI[5)], KENJI SUNAGAWA[6)]

1) Graduate School of Engineering, Tohoku University, 6-3, Aoba, Aramaki, Aoba-ku, Sendai, Miyagi 980-8578, Japan

2) Graduate School of Biomedical Engineering, Tohoku University, 6-3, Aoba, Aramaki, Aoba-ku, Sendai, Miyagi 980-8578, Japan

3) Research Division on Advanced Information Technology, Cyberscience Center, Tohoku University, 6-3, Aoba, Aramaki, Aoba-ku, Sendai, Miyagi 980-8578, Japan

4) Olympus Corporation, 2-3, Kuboyama-cho, Hachioji, Tokyo 192-8512, Japan

5) National Cerebral and Cardiovascular Center Research Institute, 5-7-1, Fujishirodai, Suita, Osaka 565-8565, Japan

6) Graduate School of Medicine, Kyushu University, 3-1-1, Maidashi, Higashi-ku, Fukuoka, Fukuoka 812-8582, Japan

The implantable cardioverter-defibrillator is an effective therapeutic device for saving patients with cardiac diseases from death caused by life-threatening arrhythmias such as ventricular tachycardia and ventricular fibrillation. It is important to prevent the recurrence and treat these arrhythmias early and to accurately distinguish between a normal sinus rhythm, ventricular tachycardia, ventricular fibrillation, and supraventricular tachycardia. Therefore, in this study, we have proposed a multiple regression model based on information extracted from simultaneous intracardiac electrocardiograms in order to identify episodes of supraventricular tachycardia, ventricular tachycardia, and ventricular fibrillation. From the experimental results, we confirmed that life-threatening arrhythmias can be detected on the basis of indices obtained from simultaneous intracardiac electrocardiograms.

Keywords: implantable cardioverter-defibrillator, arrhythmia, multiple regression model

1. Introduction

The number of victims of sudden cardiac death is estimated to be ~70,000 per year in Japan and it is increasing continuously. A sudden cardiac death is

[*] Makoto Abe was a Tohoku University Global COE Research Assistant (2007-2008).
[†] Makoto Yoshizawa is a Tohoku University Global COE Member.

directly caused by life-threatening cardiac arrhythmia such as ventricular tachycardia (VT) and ventricular fibrillation (VF). The survival rates for these arrhythmias decrease by 7–10% per minute; therefore, it is important to treat these arrhythmias early [1]. The implantable cardioverter-defibrillator (ICD) is an effective therapeutic device for saving patients with cardiac diseases from death caused by life-threatening arrhythmia. However, the traditional algorithms used in ICD for detecting VF and VT are based almost only on the information for the cardiac period [2], thus making it difficult to accurately distinguish between a normal sinus rhythm, VT, VF, and supraventricular tachycardia (SVT).

Furthermore, the incidence of inappropriate ICD treatment has not reduced. A recent study found inappropriate VT detection in 14% of patients treated for secondary sudden cardiac death prevention and in 30% of patients treated for primary prevention [3]. Another study reported positive detection of VTs using modern, optimized ICD detection algorithms in only 60–70% of patients with spontaneous tachycardias [4]. These detection errors are related to different causes; for example, ventricular oversensing causes inappropriate therapy in up to 25% of patients [3].

In order to treat VF or VT accurately, it is necessary to improve the classification algorithms that can distinguish shockable cardiac rhythms from nonshockable cardiac rhythms. In addition, these algorithms should detect arrhythmias as fast as possible.

In this study, we have proposed a method based on information extracted from intracardiac electrocardiograms (IECGs) to identify episodes of SVT, VT, and VF. IECGs were measured from the left ventricle ($IECG_{LV}$), right ventricle ($IECG_{RV}$), and right atrium ($IECG_{RA}$). The arrhythmias were classified by inputting 14 input indices obtained from these IECGs to a multiple regression model. It was possible to identify life-threatening arrhythmias within a short time with a relatively high accuracy. The proposed method was validated by performing an animal experiment.

2. Methods

2.1. *Data Description and Preprocessing*

In this study, experimental data were obtained from five dogs (*in vivo*) in an acute experiment. IECGs were measured using leads from the left and right ventricles and the right atrium. These data were sampled at 200 Hz or 1 kHz and then resampled at 250 Hz. In addition, owing to the difficulty in measuring

spontaneous arrhythmia, SVT, VT, and VF were simulated as follows. SVT was simulated by right atrial pacing. VT was simulated by right or left ventricular pacing, and VF was induced by applying electrical stimuli after the R-wave of the surface electrocardiogram. The data also included one spontaneous VF episode.

First, a bandpass filter (0.8–40 Hz) was applied to the IECG signals in order to remove the noise component. After filtering, the data were analyzed using a moving data window with a length of 1.0 s and shift of 0.2 s, as shown in Fig. 1.

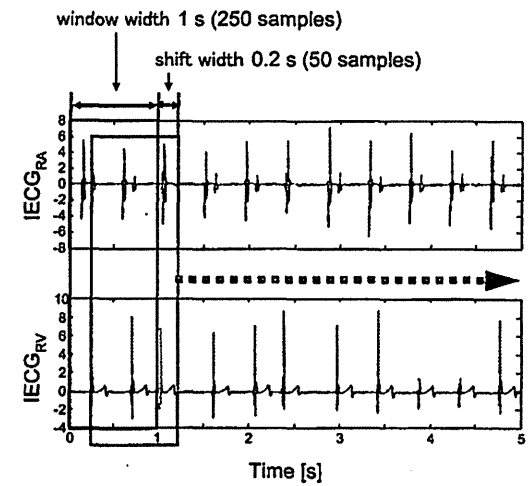

Figure 1. Data acquisition using 1-s-long window with 0.2-s shift

2.2. *Classification*

First, k is defined as the discrete time, which is increased by shifting window in every 0.2 s. Our multiple regression method is described as follows.

1. Let $x_1(k), x_2(k), \ldots, x_m(k)$ be m feature variables extracted from IECGs signal at the kth window. Define a feature vector $x(k)$ as $x(k) = [x_1(k), x_2(k), \ldots, x_m(k)]^T$.
2. Cardiac rhythms, SR, SVT, VT, and VF, are numbered from $i = 1$ to $i = 4$. The result of detection is described as follows:

$$y_i(k) = \begin{cases} 1 \text{ (if the sample belongs to the rhythm } i) \\ 0 \text{ (otherwise)} \end{cases} \quad (1)$$

Define the result of a detection vector $y(k)$ as $y(k) = [y_1(k), y_2(k), \ldots, y_4(k)]^T$.

3. Assume that the feature vector $x(k)$ is given as explanatory variable and $y(k)$ given as objective variable, a multiple regression model is described as follows:

$$y(k) = Ax(k) + e(k), \tag{2}$$

where $4 \times m$ matrix A is a regression coefficients matrix and 4×1 vector $e(k)$ is a disturbance term.

In this study, m was set to 14 and the number of windows K was set to 400 experimentally. The matrix A was calculated by the least-squares method using Equation (2). A model for each rhythm according to Equation (1) was estimated by the training dataset. The same training dataset was used for the identification of the four models of rhythms.

2.3. *Indices Based on IECGs*

2.3.1. *Histogram distribution*

In order to evaluate the index of independence between the atrial ECG and the ventricular ECG, the simultaneous frequency distribution between pairs of IECGs is expressed by five times five bins, and the Pearson's χ^2 statistic was calculated from the distribution [5]. In addition, the dispersion of the histogram was calculated as the standard deviation (σ) of the counts in each bin of the histogram.

In this study, χ^2 statistic and σ were calculated from between $IECG_{LV}$ and $IECG_{RV}$ and from between $IECG_{RA}$ and $IECG_{RV}$, which gave us the four indices extracted from the histograms.

2.3.2. *Cardiac periods*

The periods (R-R intervals) were the only indices extracted from single IECGs. In general, the cardiac period is obtained from the R-R interval using an R-wave detection method. In this study, a method with an auto-correlation function was proposed to detect the R-wave even though IECGs included much noise. The period was approximated to the time of the first peak of the auto-correlation function of each IECG in the moving 1s- window.

The cardiac periods $Period_{LV}$, $Period_{RV}$, and $Period_{RA}$ were obtained from $IECG_{LV}$, $IECG_{RA}$, and $IECG_{RV}$, respectively. In addition, we calculated the ratio between $Period_{LV}$ and $Period_{RV}$ and between $Period_{RA}$ and $Period_{RV}$.

2.3.3. *Relative delays*

The relative delay was calculated from the cross-correlation function between two IECG signals. The relative delay from $IECG_{RA}$ to $IECG_{RV}$ and that from $IECG_{RA}$ to $IECG_{RV}$ were calculated.

The relative delays and the relative periods of IECGs reflect the atrioventricular conduction. If two IECGs synchronize, the delay is almost constant. While, if two IECGs are in condition of asynchronous, the delay is inconstant. The constancy of the R-P interval is known to be a reliable diagnostic criterion for VT.

2.3.4. *Complex plain based on simultaneous distribution of IECGs*

Finally, the main angle of the distribution of two IECGs and the length of the depolarization were considered.

In order to facilitate the calculations, a complex number Z was defined as follows:

$$Z = IECG_{RV} + i \cdot IECG_{LV}, \tag{3}$$

where i is the imaginary unit. The first and third quartile points of the angle of Z were used to represent the angle of the distribution. The main angle was bigger in VT events (~80°) than in SVTs (~50°).

The length of the depolarization was approximated to the count of point of

$$|Z| > 0.05 \cdot \max_{1\,s\,window} |Z|. \tag{4}$$

In VF, the length was almost 250 (window length) because depolarization was produced during most of the cardiac cycle. On the other hand, the length was smaller in SR, when the R-R intervals are bigger, and intermediate in the tachycardia.

2.3.5. *Validation*

In order to assess the validity of the proposed method, n (from 100 to 600 every 100) windows were randomly selected for the training set and the remaining 5221 windows were used in the test set. In addition, the validation process was repeated 100 times so as to evaluate the robustness of the method.

All the indices were normalized in the training process. The same normalization coefficients were used to normalize the test set.

For the evaluation of the classifier, the area under the receiver operating characteristic (*ROCA*), the sensitivity, and the specificity were used. The closer

the *ROCA* value of the classifier is to 1, the more effective it is. The receiver operating characteristic (ROC) represents the sensitivity versus (1 - specificity) for a binary classifier system with a varying discrimination threshold. Sensitivity and specificity are defined in Eqs. (5) and (6), respectively.

$$Sensitivity = \frac{TP}{TP + FN} \tag{5}$$

$$Specificity = \frac{TN}{TN + FP}, \tag{6}$$

where *TP* is the number of true positives, *FN* is the number of false negatives, *TN* is the number of true negatives, and *FP* is the number of false positives.

3. Results

In this study, even though the classification was performed with four models, one for each rhythm, the sensitivity and specificity were calculated by considering the SVT and SR as the same class, because in both cases, the ICD was not activated.

Figures 2–4 show examples of measured signals and the corresponding output of the classifier obtained using the method described in section 2.2, before and at the beginning of different arrhythmias.

The validation results of classification by the linear regression method are listed in Table 1. Figure 5 shows the *ROCA*s of binary classification for each of the four models.

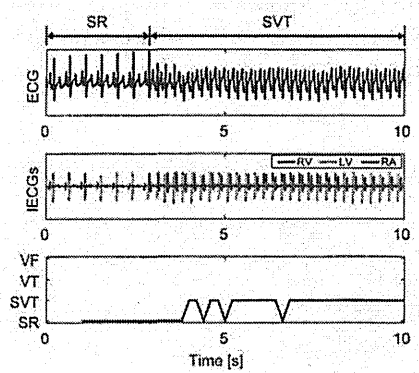

Figure 2. Example of surface ECG (top), IECGs (middle), and corresponding classifier output (bottom) at beginning of SVT episode.

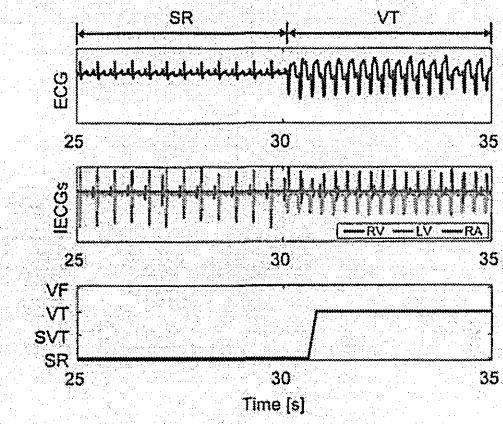

Figure 3. Example of surface ECG (top), IECGs (middle), and corresponding classifier output (bottom) at beginning of VT episode.

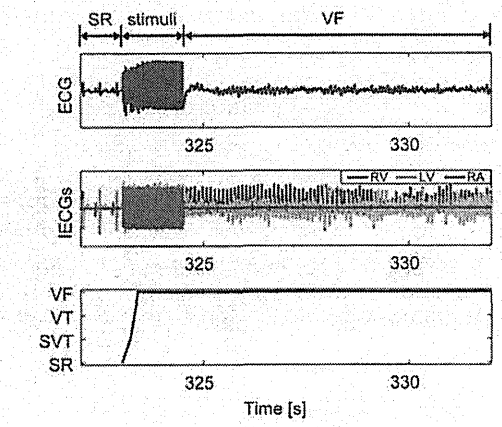

Figure 4. Example of surface ECG (top), IECGs (middle), and corresponding classifier output (bottom) at beginning of VF episode.

Table 1. Validation results for specificity and sensitivity of detection of each rhythm

	Specificity (%)	*Sensitivity* (%)
SR or SVT	98.3	96.8
VT	99.0	73.7
VF	97.4	97.4

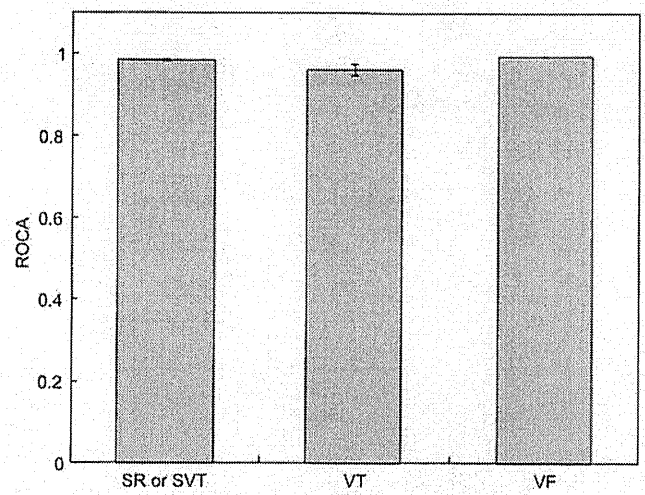

Figure 5. *ROCA* of model of each rhythm obtained from randomly selected training sets (the bars represent the mean value and the error bars represent the standard variation of *ROCA*).

4. Discussion

The results show that the proposed method could classify the cardiac rhythms SR, SVT, VT, and VF with high accuracy. In particular, Fig. 5 shows that the *ROCA* using the evaluated model was >0.94.

The use of the χ^2 statistics and σ was evaluated in a previous phase of this study [5]. These two indices enable early detection of arrhythmias; however, the accuracy of detection using only these indices is lower than that of other conventional methods, which motivated us to use additional indices for detection. Another limitation of the previous study was that only the ventricular IECGs were used, and therefore, it was difficult to distinguish between SVT and VT. Using the same dataset as in the present study, the classification proposed in the previous study resulted in the sensitivity and the specificity of, respectively, 82.7% and 80.3% for SVT or SR, 66.5% and 85.1% for VT, and 79.9% and 99.4% for VF. Most of the misclassification was SVT being classified as VT. Thus, it should be noted that this would lead to unnecessary activation of the ICD. On the other hand, in the present study, sensitivity of the detection of life-threatening arrhythmias was >73.7% and specificity was >96.8%. The low sensitivity in the detection of VTs is mostly due to the misclassification of VTs as SR or SVT.

The delay in the detection was ~1.2 s for SVTs, 1.6 s for VTs, and 1 s for VFs. Because VFs were preceded by an electrical stimulus, the delay in detection could be evaluated in only one episode. These results indicate that life-threatening arrhythmias could be detected early by using the classification based on the proposed method. This early detection is mainly attributed to the short length of the window (1s length) used to extract the selected indices.

The validation using the training set, which was randomly selected, does not guarantee a uniform distribution of each rhythm in the training set, especially of rhythms with few available data (*e.g.*, VT). This fact explains the high standard deviation in the *ROCA*s of the model of some rhythms. Furthermore, the distribution of each rhythm is not uniform in the validation set.

The main limitation of this study is that these results were obtained from a limited dataset. The algorithm should be evaluated using more data obtained under different conditions. Moreover, it is important to consider the computational and memory cost that each additional index presents.

5. Conclusion

We proposed a new algorithm for the detection of arrhythmias using ICDs. Each cardiac rhythm was classified by a multiple regression model using the indices obtained from IECG signals as inputs. The following indices were used: χ^2 statistics and standard deviation σ extracted from 2D histograms, period of each IECG and their relative ratio, delay between pairs of IECGs, main angle of distribution of two IECGs, and length of depolarization.

In the proposed method, four groups of cardiac rhythms were considered: SR, SVT, VT, and VF. The relative delay in the detection of life-threatening arrhythmias considerably affects the efficiency of the treatment. In this study, changes in the rhythms could be detected rapidly using short windows while maintaining the good performance of the classifier. The proposed method showed a sensitivity of at least 76.0% and specificity of at least 96.8% for a dataset including the data for five subjects. Thus, information from pairs of simultaneous electrocardiograms enables fast and accurate detection of arrhythmias.

Acknowledgments

Makoto Abe gratefully acknowledges the support of the Tohoku University Global COE Program: "Global Nano-Biomedical Engineering Network Centre."

References

1. American Heart Association, 2005 American Heart Association Guidelines for cardiopulmonary resuscitation and emergency cardiovascular care. *Circulation* **112**, IV-35–IV-46 (2005).
2. A. Przybylskia, R. Baranowskia, J. J. Zebrowskib and H. Szweda, Verification of implantable cardioverter defibrillator (ICD) interventions by nonlinear analysis of heart rate variability—preliminary results. *Europace* **6**, 617–624 (2004).
3. C. W. Israel, How to avoid inappropriate therapy. *Current Opinion in Cardiology* **23**, 65–71 (2008).
4. J. Gillberg, Detection of cardiac tachyarrhythmias in implantable devices. *Journal of Electrocardiology* **40**, S123–S128 (2007).
5. H. Kinoshita, M. Yoshizawa, M. Inagaki, K. Uemura, M. Sugimachi and K. Sunagawa, Development of an algorithm for detection of fatal cardiac arrhythmia for implantable cardioverter-defibrillator using a self-organizing map. In *Proceedings of the 28th IEEE EMBS Annual International Conference*, New York, 4370–4373 (2006).

SILICA COATING OF FLUORESCENT NANOPARTICLES PROLONGS ENHANCEMENT OF SENTINEL LYMPH NODES

LIMAN CONG[1)*], MOTOHIRO TAKEDA[1)], YOHEI HAMANAKA[2)†], KOHSUKE GONDA[1)], MIKA WATANABE[3)], YOSHIO KOBAYASHI[4)], MASAKI KOBAYASHI[5)], NORIAKI OHUCHI[1,2)‡]

1) Department of Nano-Medical Science, Graduate School of Medicine, Tohoku University, 2-1 Seiryo-machi, Aoba-ku, Sendai 980-8574, Japan

2) Department of Surgical Oncology, Graduate School of Medicine, Tohoku University, 1-1 Seiryo-machi, Aoba-ku, Sendai 980-8574, Japan

3) Department of Pathology, Tohoku University Hospital, 1-1 seiryo-machi, Aoba-ku, Sendai 980-8574, Japan

4) Department of Chemical Engineering, Graduate School of Engineering, Ibaraki University, Hitachi 316-8511, Japan

5) Department of Electronics, Tohoku Institute of Technology, 35-1kasumi-cho, Yagiyama, Taihaku-ku, Sendai 982-8577, Japan

Sentinel lymph node biopsy (SLNB) was developed as a new modality in the surgical diagnosis of lymph node metastases. Dyes and radioisotopes are the major tracers for the detection of sentinel lymph nodes (SLN). However, dyes tend to infiltrate excessively into the interstitium due to their small molecular size (less than several nanometers), resulting in difficulties in maintaining a clear surgical field, whereas radioisotopes are available only in a limited number of hospitals. Fluorescent nanoparticles are suitable candidates as SLN tracers in solving these problems, because we can choose a suitable particle size and near-infrared fluorescence wavelengths. However, the use of nanoparticles involves safety issues and many attempts have been made to produce insulating coats to obviate these issues. In addition, the preparation of a uniform insulating layer is important to decrease quality variations in an SLN tracer. We succeeded in coating fluorescent polystyrene nanoparticles of 40-nm size with a uniform silica layer of 13-nm thickness by the modified Stöber method. The popliteal lymph node could be visualized using silica-coated nanoparticles injected into the rat foot. The application of silica-coated fluorescent nanoparticles was demonstrated for SLN mapping in an animal model. Together, the chemical, optical, and *in vivo* data presented in this study demonstrate the potential role of silica-coated fluorescent nanoparticles for imaging in medical treatments.

Key words: sentinel lymph node, silica-coated, fluorescent nanoparticle, imaging.

---

* Liman Cong was a Tohoku University Global COE Research Assistant (2007-2008).

† Yohei Hamanaka was a Tohoku University Global COE Research Assistant (2007-2010).

‡ Noriaki Ohuchi is a Tohoku University Global COE Member.

blood

2011 118: e93-e100
Prepublished online August 5, 2011;
doi:10.1182/blood-2010-12-322842

In vivo imaging of the molecular distribution of the VEGF receptor during angiogenesis in a mouse model of ischemia

Yoh Hamada, Kohsuke Gonda, Motohiro Takeda, Akira Sato, Mika Watanabe, Tomoyuki Yambe, Susumu Satomi and Noriaki Ohuchi

Blood (print ISSN 0006-4971, online ISSN 1528-0020), is published weekly by the American Society of Hematology, 2021 L St, NW, Suite 900, Washington DC 20036.

e-*Blood*

In vivo imaging of the molecular distribution of the VEGF receptor during angiogenesis in a mouse model of ischemia

Yoh Hamada,[1,2] Kohsuke Gonda,[1] Motohiro Takeda,[1] Akira Sato,[2] Mika Watanabe,[3] Tomoyuki Yambe,[4] Susumu Satomi,[2] and Noriaki Ohuchi[1,5]

[1]Department of Nano-Medical Science, Graduate School of Medicine, Tohoku University, Sendai, Japan; [2]Department of Advanced Surgical Science and Technology, Graduate School of Medicine, Tohoku University, Sendai, Japan; [3]Department of Pathology, Tohoku University Hospital, Sendai, Japan; [4]Department of Medical Engineering and Cardiology, Institute of Development, Aging and Cancer, Tohoku University, Sendai, Japan; and [5]Department of Surgical Oncology, Graduate School of Medicine, Tohoku University, Sendai, Japan

Vascular endothelial growth factor (VEGF) plays a critical role in angiogenesis and has been applied to medical therapy. However, because vascular imaging at the molecular level is impossible, the detailed in vivo dynamics of VEGF and its receptor (VEGFR) remain unknown. In this study, to understand the molecular distribution of VEGF and the VEGFR, we prepared ischemic mice with a new surgical method and induced angiogenesis in the gastrocnemius muscle. Then, we made a VEGF-conjugated fluorescence nanoparticle and performed staining of VEGFR-expressing cells with the fluorescent probe, demonstrating the high affinity of the probe for VEGFR. To observe the physiologic molecular distribution of VEGFR, we performed in vivo single-particle imaging of gastrocnemius in the ischemic leg with the fluorescent probe. The results suggested that only a 3-fold difference of VEGFR distribution is involved in the formation of branched vasculature in angiogenesis, although previous ex vivo data showed a 13-fold difference in its distribution, indicating that a method inducing a several-fold local increase of VEGFR concentration may be effective in generating site-specific angiogenesis in ischemic disease. This new in vivo imaging of ischemic mice could make useful contributions to understanding the mechanisms of angiogenesis and to developing a VEGFR-related drug. (*Blood*. 2011;118(13): e93-e100)

Introduction

Angiogenesis and arteriogenesis play a critical role in neovascularization in adults.[1] Angiogenesis is defined as the sprouting of new capillaries from postcapillary venules,[2] whereas arteriogenesis is defined as the process of artery maturation or the de novo growth of collateral conduits.[3] Our laboratory studies the mechanisms of angiogenesis, and clarification of these mechanisms is crucial for the development of new treatments for arteriosclerotic disorders. Recently, medical applications for recombinant vascular endothelial growth factor (VEGF) proteins or genes have been developed.[4] However, no placebo-controlled trial has yielded overwhelmingly positive results.[1] An understanding of the detailed molecular mechanisms of this angiogenesis factor in vivo is thought to be very important for the effective design of a VEGF-related drug delivery system. However, neither VEGF activity nor VEGFR distribution has been quantitatively analyzed in vivo at a molecular level with respect to therapeutic angiogenesis. In previous animal studies, the efficacy of treatment for atherosclerotic disease was primarily evaluated using angiography, laser Doppler imaging, and the determination of histologic capillary density.[5,6] Angiography can be used to noninvasively visualize vessel size, vessel branching, and the vascular network throughout the body. However, because it is difficult to visualize vascular structures several hundred micrometers beneath the imaging surface, this method is not adequate for the observation of early-stage angiogenesis at a molecular level. Laser Doppler imaging provides a noninvasive measurement of blood flow by determining the Doppler frequency shift of reflected light because of the motion of red blood cells. This technique enables quantitative analysis of improvements in blood flow after injury to the vasculature. However, the Doppler shift measurement is easily influenced by movement artifacts, room temperature, and blood pressure.[7] In addition, it is difficult to analyze microvascular structures using laser Doppler imaging because the resolution of the obtained image is limited by diffusion of the reflected light because of distance between the red blood cells and the detector. Histologic measurements of capillary density can reveal quantitative increases in blood vessel density, and many previous studies have used this metric as a standard evaluation of angiogenesis. However, continuous observation of the same tissue is impossible with this measurement technique as protein structure is influenced by fixation of the tissues. For this reason, histologic techniques are not recommended for physiologic observations of the angiogenesis process. In the aforementioned methods, as resolution is limited to the micrometer level and imaging at the molecular level is currently impossible, the detailed in vivo dynamics of individual VEGF and VEGF receptor (VEGFR) molecules remain unknown. We have developed an in vivo single-particle imaging system using bright and photo-stable fluorescent nanoparticles, or quantum dots (QDs), with a spatial

Submitted December 2, 2010; accepted July 25, 2011. Prepublished online as *Blood* First Edition paper, August 5, 2011; DOI 10.1182/blood-2010-12-322842.

The online version of this article contains a data supplement.

The publication costs of this article were defrayed in part by page charge payment. Therefore, and solely to indicate this fact, this article is hereby marked "advertisement" in accordance with 18 USC section 1734.

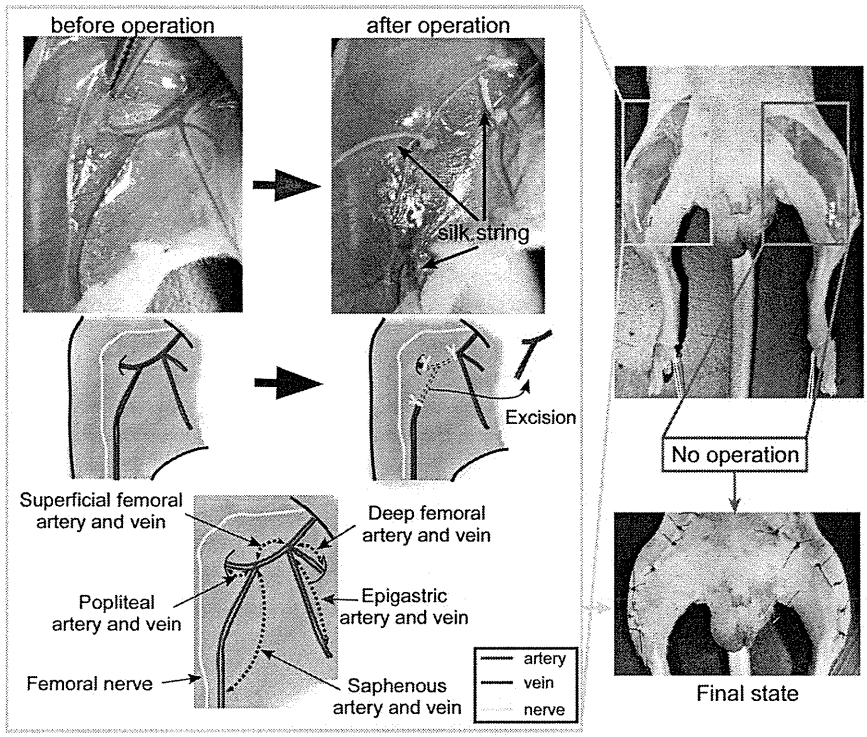

Figure 1. Procedure for preparing the hemi-hind limb ischemic mouse model. On the right leg, we ligated the proximal end of the superficial femoral artery and vein, the origins of the popliteal artery and vein, and the distal portions of the saphenous artery and vein with surgical silk. All vessels surrounding the 3 ligated points were excised. The left leg was not treated, except for an incision in the skin of the thigh.

precision of 7-9 nm. This was performed to clarify the molecular mechanisms of an anti-HER2 antibody-based drug delivery system and of cancer metastasis in tumor-bearing mice.[8,9]

The use of an ischemic mouse model is highly effective for understanding the in vivo molecular dynamics of angiogenic factors and their effects on vascular remodeling. However, 2 surgical concerns impose limitations on previous mouse models.[10] First, angiogenesis and arteriogenesis were not separately evaluated in previous models. As both processes contribute to an increase in the rate of blood flow,[1] it is necessary that the effects of arteriogenesis be eliminated if angiogenesis is to be analyzed. Second, inflammation and edema at the surgical site are known to affect angiogenesis.[11] To overcome these problems, it is critical to establish an improved ischemic mouse model that selectively induces angiogenesis at a specific muscle. Here, we demonstrate the development of an imaging method for determining the molecular distribution of VEGFR labeled with QD-conjugated VEGF. This technique was designed to observe angiogenesis in a novel ischemic mouse model that induces angiogenesis in the gastrocnemius. Our results suggest that only a several-fold difference in VEGFR distribution is required for the promotion of angiogenesis. This novel imaging method may aid in the development of drugs and treatments for atherosclerotic diseases.

Methods

Animals

C57BL/6J male mice (Charles River Laboratories) weighing 20-27 g and 8-9 weeks of age were used for all experiments. All surgical processes were performed under anesthesia with ketamine (100-120 mg/kg) and xylazine (8-10 mg/kg). Anesthesia was maintained for the course of the imaging session. Animals were used in accordance with guidelines approved by the committee on animal experiments of Tohoku University.

Hemi-hind limb ischemic mouse model

The hair of each mouse was removed from the abdomen and both hind limbs with an electric shaver and depilatory cream. The skin from both thighs was then incised to expose the arteries, veins, and nerves. To induce selective ischemia in the gastrocnemius, which is located in the deep layer of the thigh muscles, 3 vessels of the femoral area were ligated in the right hind limb. First, the proximal end of the superficial femoral artery and vein were ligated with surgical silk, size 6-0. Second, the origins of the popliteal artery and vein were ligated. Third, the distal portions of the saphenous artery and vein were ligated to avoid the backflow of blood. Femoral nerves were carefully preserved. Each of the vessels that were surrounded by the 3 ligated points was excised. The left leg was not treated, except for an incision in the skin of the thigh. Finally, the overlying skin was closed (Figure 1).

Histologic capillary density

To confirm that the surgical operation-induced angiogenesis in the gastrocnemius, we performed immunohistologic staining of the muscle with anti-CD31 antibody, a marker for vascular endothelial cells. Mice were killed at predetermined times (7, 14, 21, and 28 days after operation). The gastrocnemius was removed and fixed overnight in 10% formalin in PBS. After fixation, the tissue was embedded in paraffin, and the tissue sections were prepared and mounted on slides. The tissue samples were deparaffinized, and antigen retrieval was performed with proteinase K treatment. After this treatment, the tissue samples were incubated with a rat anti-CD31 monoclonal primary antibody (Angio-Proteomie) at 5 μg/mL for 12 hours at 4°C. After being washed with PBS, the samples were incubated with a biotinylated antirat IgG secondary antibody (Vector Laboratories; 100-fold dilution) for 30 minutes at 25°C. After incubation, the samples were incubated with HRP-conjugated streptavidin (Nidchirei) for 30 minutes at 25°C. Samples were then treated with diaminobenzidine chromogen reagent (Dojindo) and counterstained with hematoxylin. The samples were observed using light microscopy (BX51; Olympus) with an objective lens (×40, 0.75 NA; Olympus) and a camera (DP-25B; Olympus). The images were acquired with image processing software (DP2-BSW Version 1.2).

Laser Doppler perfusion imaging

Blood perfusion of the hind limb was measured using a Laser Doppler Perfusion Imaging system (MoorLDI2-IR; Moor Instruments). This imaging technique provides a noninvasive measurement of blood flow by determining the Doppler frequency shift of light reflected off of moving red blood cells. Mice under the same anesthetic dose described in "Animals" were scanned from the lower abdomen to the end of the toes. After scanning, colored images were obtained with original software (RESEARCH Version 3.09; Moor Instruments). Each pixel in the acquired images reflected an original blood flow value, referred to as a perfusion unit (PU). The mean of the PUs of the lower thighs in a control limb and a treated hind limb was determined. The PUs of ischemic legs were obtained at different time points (before operation, soon after operation, and 7, 14, 21, and 28 days after operation). The relative ratios of the mean PUs between the ischemic and control legs in the same mouse were calculated.

Cell lines

A pancreatic islet endothelial mouse cell line, MS1, was obtained from ATCC. MS1-VEGF cells, which express VEGFR on the cell membrane via the transfection of the VEGF gene, were also acquired from ATCC. These cells were cultured in DMEM (Invitrogen) supplemented with 5% FBS.

Immunostaining of cultured cells with an anti-VEGFR antibody

MS1 and MS1-VEGF cells were cultured on slide glass chambers. After 3 days, the slides were placed in 2.5% formalin in DMEM for 10 minutes. After fixation, the cells were incubated with an anti–mouse VEGFR monoclonal antibody (Pierce Chemical) or a whole mouse IgG (Rockland) primary antibody at 10 μg/mL for 12 hours at 25°C. After the samples were washed with PBS, the cells were incubated with a HRP-conjugated anti–mouse IgG secondary antibody (KPL Europe; 100-fold dilution) for 1 hour at 25°C. After incubation, the samples were treated with diaminobenzidine chromogen reagent and counterstained with hematoxylin. We observed the samples with the same optical system in "Histologic capillary density."

Preparation of angiogenesis factor-conjugated QDs

Mouse VEGF 164 (R&D Systems) and platelet-derived growth factor BB (PDGF; Biovision) were biotinylated using the EZ-Link Micro Sulfo-NHS-LC-Biotinylation Kit (Pierce Chemical). In this reaction, a 1:50 molar ratio of angiogenesis factors and Sulfo-NHS-LC-Biotin was used according to the manufacturer's instructions. The biotinylated VEGF and PDGF were then mixed with avidin-conjugated Qdot705 nanoparticles (QD705; Invitrogen) at a molar ratio of 8:1 or 16:1 and incubated for 1 hour at 25°C. The number of QD705 nanoparticles determined the emission wavelength. QD705-conjugated VEGF and PDGF were termed VEGF-QD and PDGF-QD, respectively.

Single-particle imaging system

The optical system used to observe the fluorescence of the angiogenesis factor-conjugated QDs consisted primarily of an epifluorescent microscope (IX-71; Olympus), a Nipkow disk-type confocal unit (CSU10; Yokogawa), and an EMCCD camera (Ixon DV887; Andor). An objective lens (60×, PlanApo, 1.40 NA; Olympus) was used for imaging. VEGF-QDs were illuminated using a green laser (532 nm; Spectra-Physics). The laser-excited fluorescence of the QDs was filtered with a 695- to 740-nm band-pass filter. Images were obtained at a rate of 5 frames/second. For in vivo imaging, to remove the oscillation because of heartbeats and respiration, a gastrocnemius window was developed and attached to the aforementioned microscopy system.

Single-particle imaging of VEGF-QDs in cultured cells

To investigate the affinity of VEGF-QDs for VEGFR, MS1, and MS1-VEGF, cells were incubated with 1, 10, or 50nM VEGF-QDs for 1 hour at 25°C. After 3 washes with DMEM, these cells were observed in a glass-bottom dish using the single-particle imaging system. The fluorescence intensities of QD signals from the cells were analyzed as gray values using ImageJ 1.38 software (www.rsb.info.nih.gov/ij). The gray values of 100 frames (200 milliseconds/frame) from a single cell were averaged, and the gray value of the background was subtracted from that of the cell. The mean gray value per pixel in the background-subtracted image of the cell was multiplied by the total number of pixels making up the image of the cell. The total fluorescence intensity of the QDs per cell was thus determined. In the 10nM VEGF-QD treatment, QD fluorescence signals were clearly observed on MS1-VEGF cells. In contrast, when MS1-VEGF cells were incubated with 1nM VEGF-QDs, the QD fluorescence signals were low. When the cells were treated with 50nM VEGF-QDs, QD signals were exceedingly high or even saturated (data not shown). In MS1 cells incubated with various concentrations of VEGF-QDs, the VEGF-QD fluorescence signals were very low. These results indicate that VEGF-QDs specifically recognize VEGFR and that the 10nM concentration was appropriate for imaging the binding of VEGF-QDs to VEGFR. Moreover, to provide stronger evidence of the affinity of VEGF-QDs for VEGFR, MS1, and MS1-VEGF, cells were incubated with 10nM unconjugated QDs, PDGF-QDs, or VEGF-QDs for 1 hour at 25°C, and the resulting fluorescence intensities were examined.

In vivo fluorescence imaging with the IVIS Spectrum system

To confirm that VEGF-QDs accumulated in the ischemic leg, we performed in vivo fluorescence imaging using the IVIS Spectrum imaging system (Caliper Life Sciences) at 4, 9, and 14 days after preparation of ischemic model mice. Unconjugated QDs or VEGF-QDs were injected intracardially into the mice. The final concentration of the QD probes in the blood was 10nM, as determined by the single-particle imaging data from cultured cells. The detection sensitivity of the fluorescent signal using the IVIS Spectrum is poorer than the single-particle imaging system but allows for noninvasive visualization of the whole body of the mouse. Therefore, fluorescence images were taken 10 minutes after injection of fluorescent probes, before the fluorescence signals decreased, because of their washing out with the blood. Fluorescence intensities of the QDs were analyzed using accessory software (Living Image Version 4.0; Caliper Life Sciences). For data analyses, the relative ratio of fluorescence between the ischemic and control leg of the same mouse was calculated.

Single-particle imaging of VEGF-QDs in the gastrocnemius of ischemic model mice

To examine the distribution of VEGF-QDs in the gastrocnemius of the ischemic leg, we performed in vivo single-particle imaging of the vasculature 4, 9, and 14 days after operation. The skin of the ischemic leg was opened to expose the thigh muscles. The skin of the hind limbs was then fixed to a plastic plate using suture thread and Superglue. Use of Superglue made both connections of the skin to the plate more stable without damaging the vasculature, eliminating the background oscillations from the heartbeat and respiration during observation. To expose the gastrocnemius, the skin and hemimembranous muscle, which is located on the superficial layer of the gastrocnemius, were then removed. The mouse, which was mounted as described on the plastic plate, was then fixed to a hand-made aluminum stage designed to stabilize the plate with screws. Unconjugated QDs or VEGF-QDs were injected intracardially into the mice. The sensitivity of the single-particle imaging system to the fluorescence signal is extremely high; and immediately after injection, a part of probes are free in the blood and have not bound to VEGFR. This initially prevents observation of the interaction between the VEGF-QDs and VEGFR on the vascular wall. Therefore, in vivo single-particle imaging of the fluorescent probes was carried out 1 hour after injection. By this time, the concentration of the free probe in the blood was decreased. To quantitatively measure the affinity of the VEGF-QDs for the vasculature, an analysis was performed as follows. A total of 100 frames, each 512 pixels square and representing an exposure of 200 milliseconds, were overlaid using image processing software (G-count 1.01; G-angstrom). A portion of the overlaid (192 pixels square) image was examined to determine the number of QD particles in proper-sized vasculature. For each image analyzed, the fluorescence intensity (as gray values) of QD signals from the tissues was determined using ImageJ software. The mean gray value, derived from the tissues'

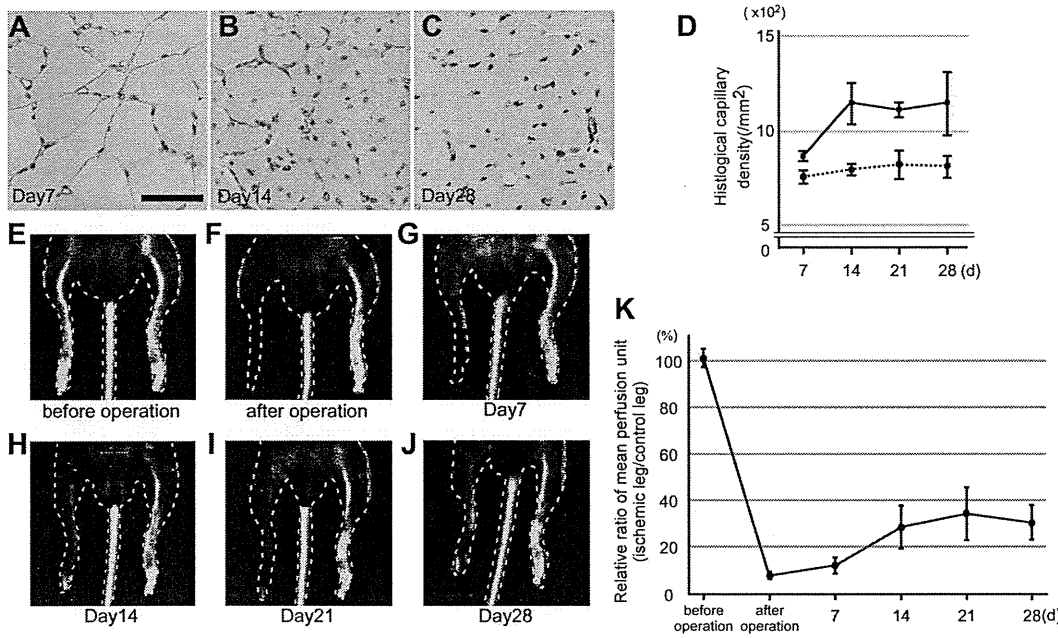

Figure 2. Evaluation of angiogenesis of the ischemic model mice. (A-C) Typical images of the gastrocnemius immunostained with an anti-CD31 antibody. The muscles from ischemic legs were isolated at 7, 14, and 28 days after the induction of ischemia and immunostained. Brown circles and dots represent $CD31^+$ capillaries. Scale bar represents 50 μm. (D) Measurement of $CD31^+$ capillary density. In the gastrocnemius of the ischemic or control leg, capillaries stained with the anti-CD31 antibody were counted. Solid and dotted lines represent the sample derived from ischemic and control legs, respectively. n = 4. Error bars represent SEM. (E-J) Changes in blood perfusion were assessed using laser Doppler perfusion imaging in ischemic legs of model mice. (E-F) Images before and soon after operation. After operation, the perfusion signal in the ischemic leg is significantly decreased. (G-J) Images from 7, 14, 21, and 28 days after operation. Blood perfusion in an ischemic leg gradually increases. (K) Change in perfusion units as determined by this imaging technique. Relative ratios of mean perfusion units between ischemic and control legs in the same mouse are shown (ischemic leg value/control leg value). n = 6. Error bars represent SEM.

autofluorescence per pixel, was subtracted from the fluorescence value of the vascular wall area. The resulting gray value was then multiplied by the total number of pixels of the vascular wall. This value reflected the total fluorescence intensity of all QDs bound to the vascular wall (total QD value).

To precisely determine the number of QD particles on the vascular wall, it was necessary to define the fluorescence intensity of a single QD. Because QDs that fluoresce at the same wavelength are uniform in size, QD705 fluorescence intensity is proportional to the particle number. Moreover, the QD fluorescence is composed of fluorescent and nonfluorescent states referred to as on- and off-states. This property results in blinking of a QD. When the fluorescence and other properties of QD particles were analyzed immediately after their purchase, we determined that the mean duration of the off-state over 20 seconds was approximately 4 seconds and that the calculated SEM was very low.[12] In cases where QDs aggregate, the mean duration of the off-state per unit time is shortened because the on- and off-states of each particle in the aggregate occur randomly. Therefore, based on an off-state duration of 4 seconds, we selected a single particle QD from each image and measured the fluorescence intensity of the single QD particle (single QD value) in the same manner as the total QD value. The total QD value was divided by a single QD value, and the number of QD particles per 10 μm of vascular wall was calculated.

Statistical analysis

Data are mean ± SEM. An F test was performed and equal variance was defined as P values ≥ .05. Comparisons between groups were performed using the parametric Student t test (≥ .05 at F test) or Welch t test ($P < .05$ at F test). $P < .05$ was considered significant for both t tests.

Results

Induction of angiogenesis in ischemic model mice

To induce angiogenesis at a selected site and to eliminate the effects of inflammation and edema,[11] we targeted the gastrocnemius. This muscle is primarily supplied by the popliteal and saphenous arteries, and no remarkable collateral arteries exist near the muscle. We therefore ligated the popliteal and saphenous arteries to induce angiogenesis in the gastrocnemius (Figure 1). Other muscles in the thigh are primarily supplied by the deep femoral artery, which was maintained as a collateral artery after the surgery. Therefore, we think that our surgery is appropriate for analyses of angiogenesis mechanisms. The gastrocnemius is located deep among the thigh muscles, and the skin and semimembranosus muscle located on the upper layer of the gastrocnemius were removed just before in vivo imaging. Therefore, we avoided the effects of inflammation and edema-induced factors on normal angiogenesis. To determine whether the number of capillaries in the gastrocnemius of ischemic legs increased, we histologically determined the capillary densities over time (Figure 2A-C). Capillary densities in the control legs did not significantly change during observation (Figure 2D). In contrast, the capillary densities in ischemic legs increased gradually over 14 days, peaked at day 14, and were steady between day 14 and day 28. This finding demonstrates that angiogenesis was induced in the ischemic leg (Figure 2D). To investigate improvement of blood flow in the model mice using another method, we evaluated the change in blood flow using laser Doppler perfusion imaging (Figure 2E-J). The relative ratio of the mean PU between ischemic and control legs in the same mouse (ischemic leg value/control leg value) decreased to ~ 8% soon after operation (Figure 2E-F,K). This ratio then increased to ~ 34% 21 days after the surgery (Figure 2I,K). Both observations indicate that angiogenesis was effectively induced in the gastrocnemius between 7 days and 14 days after the procedure. The slight difference in the rate of increase of perfusion between the 2 imaging methods may be because the laser Doppler perfusion imaging analyzed the thigh as a whole, and arteriogenesis induced by inflammation and

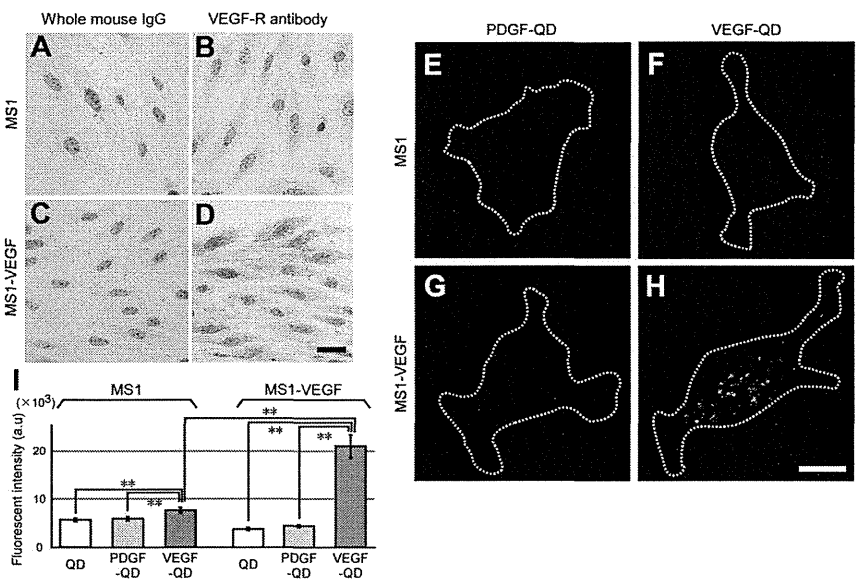

Figure 3. VEGFR distribution in MS1 and MS1-VEGF cells and the affinity of angiogenesis factor-conjugated QDs to these cell lines. (A-D) Immunostaining of MS1 and MS1-VEGF cells with an anti-VEGFR antibody. Scale bar represents 50 μm. (E-H) Typical images of cells treated with fluorescent particles. MS1 and MS1-VEGF cells were treated with unconjugated QDs, PDGF-QDs, or VEGF-QDs. Representative images are shown of cells treated with PDGF-QDs and VEGF-QDs. Data from cells treated with unconjugated QDs are not shown. White dots represent fluorescent QDs; and white dotted lines, the outline of the cell. Scale bar represents 10 μm. (I) QD fluorescence intensity per cell. The fluorescence intensity of QD signals from the cells was analyzed as gray values. In each condition, n = 30. $^{**}P < .01$. Error bars represent SEM.

edema of the semimembranous muscle may have occurred in this larger volume.

Preparation and characterization of VEGF-QDs

To visualize the molecular distribution of VEGF using single-particle imaging, VEGF was conjugated with QDs (VEGF-QD). PDGF-conjugated QDs (PDGF-QD) were also prepared as control probes (supplemental Figure 1, available on the *Blood* Web site; see the Supplemental Materials link at the top of the online article). To examine the binding of VEGF-QD and VEGFR, staining was performed on MS1 and MS1-VEGF cells treated with unconjugated QDs, PDGF-QDs, and VEGF-QDs. High levels of VEGFR expression in MS1-VEGF cells were confirmed by immunostaining with an anti-VEGFR antibody (Figure 3C-D), whereas low-level expression was observed in MS1 cells (Figure 3A-B). The analyses of QD-probe fluorescence indicated that the total fluorescence intensity of VEGF-QDs in MS1-VEGF cells was $21.0 \pm 2.4 \times 10^4$ (Figure 3H-I). This value was remarkably higher than the observed fluorescence values of stained MS1-VEGF cells treated with unconjugated QDs or PDGF-QDs (unconjugated QDs, $3.8 \pm 0.3 \times 10^4$; PDGF-QDs, $4.4 \pm 0.3 \times 10^4$; Figure 3G,I) and those of MS1 cells treated with unconjugated QDs, PDGF-QDs, or VEGF-QDs (unconjugated QDs, $5.7 \pm 0.4 \times 10^4$; PDGF-QDs, $6.0 \pm 0.4 \times 10^4$; VEGF-QDs, $7.7 \pm 0.6 \times 10^4$; Figure 3E-F,I). These results demonstrate that VEGF-QDs bind specifically to VEGFR.

In vivo distribution of VEGFR labeled with VEGF-QDs

To determine the distribution of VEGFR labeled with VEGF-QDs during angiogenesis, we performed 2 in vivo fluorescence imaging techniques. In these imaging protocols, we examined ischemic model mice at 4, 9, and 14 days after operation to analyze in detail the changes in VEGFR distribution over time. Imaging performed with the IVIS Spectrum system has the advantage of imaging the fluorescence of the entire body of the mouse, although the spatial precision of this technique is low. To simultaneously observe the fluorescence of both ischemic and control legs after injection of unconjugated QDs or VEGF-QDs into the model mice, the IVIS Spectrum system was used (Figure 4A-D). Individual mice exhibit different degrees of autofluorescence. The relative ratio of fluorescence between the ischemic and control leg in each mouse was therefore calculated (ischemic leg fluorescence/control leg fluorescence). In model mice at 4 days after operation, the relative fluorescence ratio resulting from injection of unconjugated QDs was 0.71 ± 0.01, and the ratio after injection of VEGF-QDs was 0.72 ± 0.03 (Figure 4E). These results indicate that VEGF-QDs did not selectively accumulate in the ischemic legs at the time of

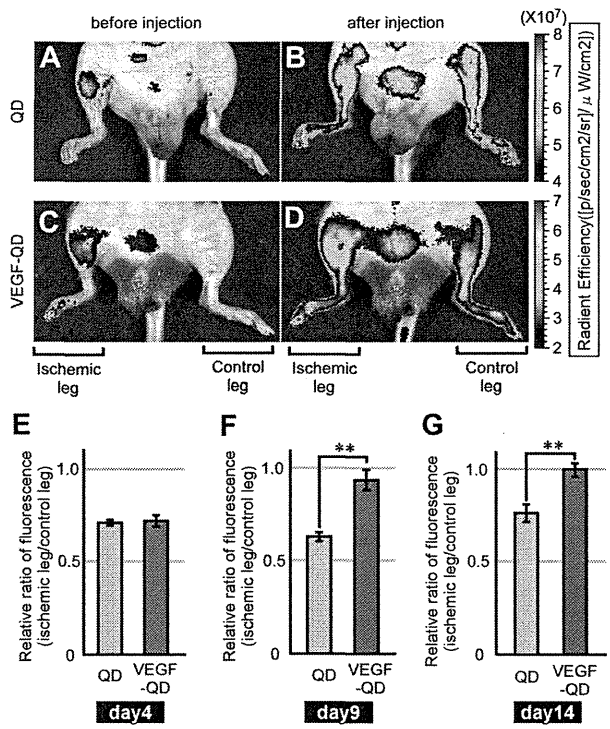

Figure 4. In vivo fluorescence imaging of the ischemic model mice using the IVIS Spectrum system. (A-D) Images using IVIS Spectrum. Unconjugated QDs and VEGF-QDs were injected intracardially into the model mice. Mice were illuminated with light with a wavelength of 625-655 nm. Excited fluorescence was filtered with a 690- to 710-nm wavelength band-pass filter. (E-G) The relative ratios of fluorescence between ischemic and control legs in mice at 4 days (E), 9 days (F), and 14 days (G) after operation. The fluorescence intensity of the ischemic leg divided by that of the control leg was calculated (ischemic leg fluorescence/control leg fluorescence). n = 5. Error bars represent SEM. $^{**}P < .05$.

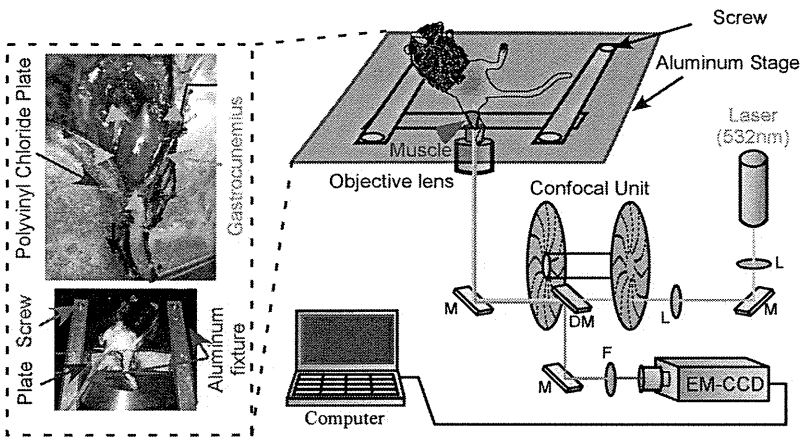

Figure 5. Schematic of the in vivo single-particle imaging system. An ischemic leg of a model mouse was stabilized on a polyvinyl plate using suture thread and instant Superglue. The skin and hemimembranous muscle were then removed. The gastrocnemius was selectively imaged using a single-particle imaging system.

measurement. In contrast, at 9 and 14 days after operation, the relative ratios resulting from injection of unconjugated QDs were 0.65 ± 0.02 and 0.76 ± 0.05, respectively, whereas the observed ratios after injection of VEGF-QDs were 0.94 ± 0.06 and 1.00 ± 0.04, respectively (Figure 4F-G), suggesting that VEGF-QDs accumulated in the ischemic leg to a greater degree than in the control leg at the time of measurement.

In addition to using the IVIS system, we also conducted in vivo single-particle imaging. For this protocol, we developed surgical fixation methods of mice beyond that in our previous imaging method. In particular, we designed a polyvinyl chloride plate with a window fit to the shape of the gastrocnemius. The skin around the gastrocnemius was bound to the plate with suture thread and Superglue (Figure 5). These improvements eliminated background oscillations because of the heartbeat and respiration, enabling us to observe the physiologic angiogenesis that sustains blood flow after ischemia (supplemental Movies 1, 2). We observed the distribution of unconjugated QDs or VEGF-QDs after injection of the respective probe. The results indicate that a large number of VEGF-QDs were specifically localized on the vessel walls in ischemic legs (Figure 6A-H), whereas fluorescence after injection of unconjugated QDs was very weak (supplemental Figure 2A-D). We measured the total fluorescence intensity resulting from all QDs on the vascular wall (total QD value) and the fluorescence intensity of single QD (single QD value) as gray values. The total QD value was then divided by the single QD value, and the number of QD particles per 10 μm of the vascular wall was calculated (Figure 6I; supplemental Figure 2E). These analyses revealed that QD fluorescence on the vascular wall was weak in both ischemic and control legs in mice injected with unconjugated QDs (supplemental Figure 2E). When VEGF-QDs probe were injected at 4 days after operation, the number of VEGF-QDs on the vascular walls of ischemic legs was similar to the number observed in control legs. Moreover, there was no difference in number of particles on the walls of branched or linear vasculature in ischemic legs (Figure 6C-D,I). In contrast, the number of VEGF-QDs in the branched vasculature in ischemic legs was 3.4-fold greater than the number of VEGF-QDs in the linear vasculature 9 days after operation (Figure 6E-F,I) and 4.5-fold greater than the number of VEGF-QDs in the branched vasculature in control legs (Figure 6B,F,I). Fourteen days after operation, the number of VEGF-QDs on the walls of the branched vasculature in ischemic legs was 3.3-fold greater than the number of particles on the walls of the linear vasculature (Figure 6G-I) and 4.3-fold greater than the number of VEGF-QDs in the branched vasculature in control legs (Figure 6I). These results demonstrate that our single-particle imaging method is able to quantitatively describe the in vivo distribution of VEGFR labeled with VEGF-QDs during angiogenesis in ischemic legs.

Discussion

In vivo molecular imaging using high spatial precision in ischemic model mice is highly effective for the quantitative description of the molecular dynamics of VEGF and VEGFR during angiogenesis. This information can be applied to the development of treatments for ischemic disease. Previously described mouse models suffered from surgical limitations. These difficulties involved: (1) the induction of angiogenesis without arteriogenesis, an effect of arteries that remains after surgery; and (2) the induction of inflammation and edema during surgery.[10] We focused on the gastrocnemius, which is located deep in the thigh, and developed a new ischemic mouse model consisting of the ligation of 3 pairs of vessels: the superficial femoral, popliteal, and saphenous arteries and veins (Figure 1). We confirmed that angiogenesis was effectively induced in the model mice using conventional evaluation methods, histological capillary density measurements, and laser Doppler imaging (Figure 2D,K).

We have previously described the development of in vivo single-particle imaging using QDs with a spatial precision of 7-9 nm to clarify the molecular mechanisms of a anti-HER2 antibody-based drug delivery system and cancer metastasis in tumor-bearing mice.[8,9] In previous studies, in vivo imaging with high spatial precision was not applied to the visualization of angiogenesis. For this application in the current studies, we further modified our surgical fixation method (Figure 5). For the imaging technique used here, we designed a polyvinyl chloride plate with a window fit to the shape for the gastrocnemius. This window enabled us to observe the physiologic angiogenesis during active blood flow. We observed the in vivo molecular distribution of VEGF-QDs using this improved imaging in ischemic mice at 4, 9, and 14 days after a surgery in which angiogenesis in the gastrocnemius was effectively induced. The results demonstrate that a large number of VEGF-QDs specifically localized to the vessel wall in ischemic legs (Figure 6A-H), whereas fluorescence resulting from unconjugated QDs at the wall was very weak (supplemental Figure 2A-D). To quantitatively analyze the molecular distribution of VEGF-QD-labeled VEGFRs, we measured the total number of QDs

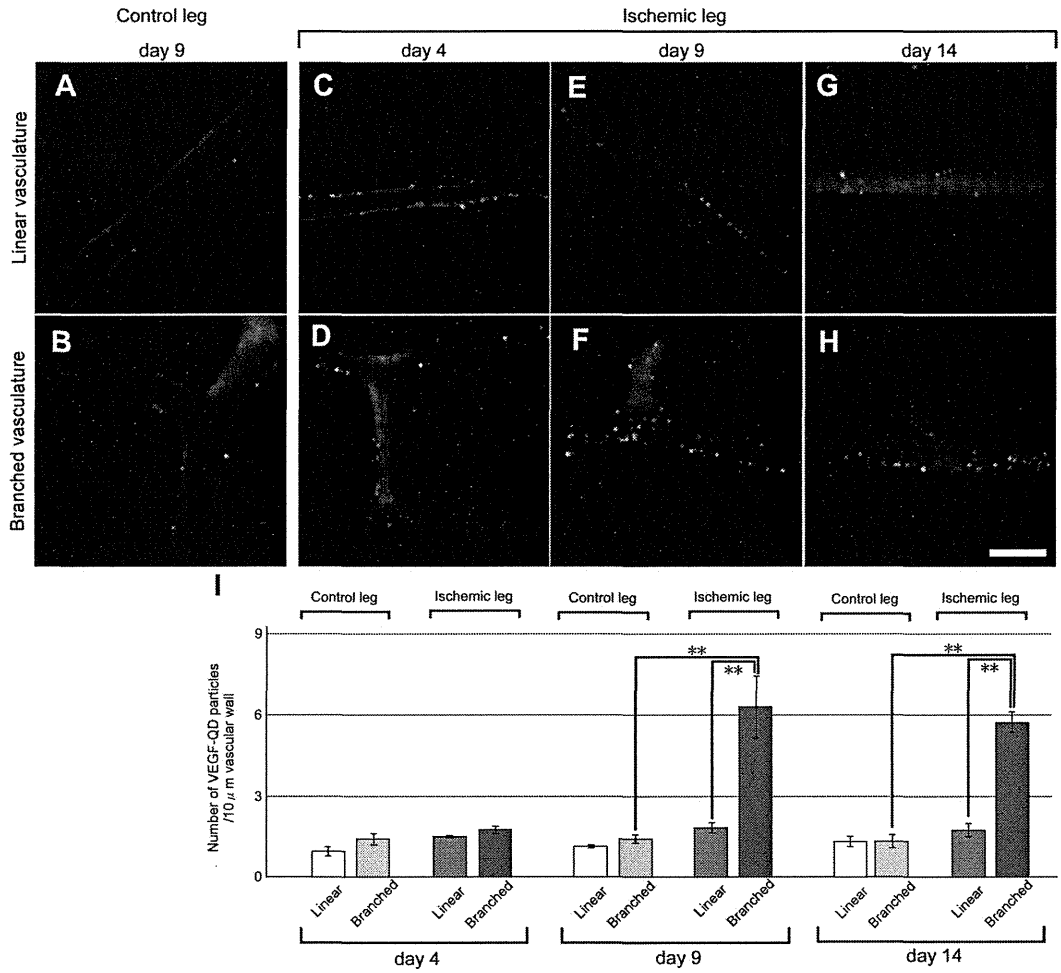

Figure 6. In vivo imaging of unconjugated and VEGF-QDs during angiogenesis in ischemic legs. (A-H) Typical images of vasculature in control and ischemic legs. These images were generated by overlaying 100 frames (200 ms/frame), each consisting of a 192-pixel square image, using Adobe after effect CS4 9.0.3 software. In model mice injected with VEGF-QDs, we observed "linear vasculature" (A,C,E,G) and "branched vasculature" (B,D,F,H) in control and ischemic mouse legs at 4, 9, and 14 days after operation. The data from unconjugated QDs are not shown (supplemental Figure 2). White dots represent QD fluorescence. Scale bar represents 10 μm. (I) The number of VEGF-QDs in different types of vasculature. The number of fluorescent particles per 10 μm of the vascular wall is quantified. n = 4. $^{**}P < .05$. Error bars represent SEM.

(Figure 6I; supplemental Figure 2E). Because QDs with the same fluorescence wavelength are uniform in size, the fluorescence intensity of the QDs is proportional to the number of particles.[12] This property enabled us to determine relative VEGFR expression levels with a very high degree of accuracy. In mice 4 days after operation, there were no significant differences between the branched vasculature and the linear vasculature (Figure 6C-D,I). Furthermore, the IVIS Spectrum data from this time point did not show a significant difference in the accumulation of unconjugated QDs or VEGF-QDs in ischemic legs (Figure 4E). These data indicate that any VEGFR redistribution induced by hypoxic stimulation in ischemic legs occurs only at low levels at this time point. In mice at 9 days after operation, the data demonstrate a 3.4-fold greater number of VEGF-QDs on the walls of branched vasculature in ischemic legs than on the walls of linear vasculature in these legs and a 4.5-fold greater number than on the branched vasculature of control legs in model mice (Figure 6I). In mice at 14 days after operation, the data revealed that the number of VEGF-QDs on the walls of branched vasculature in ischemic legs was 3.3-fold greater than that on the linear vasculature in ischemic legs and 4.3-fold greater number than the number of VEGF-QDs on the branched vasculature in control legs in model mice (Figure 6I). These results demonstrate that the data acquired from mice at 9 and 14 days after operation using the single-particle imaging technique were similar to data acquired using the IVIS Spectrum system (Figure 4F-G). From the data, it appears that the VEGFR protein expression on the branched vasculature in ischemic legs increases gradually between day 4 and day 9 via hypoxic stimulation, peaks at approximately day 9, and remains steady from day 9 to day 14. Histologic capillary density data reveal that capillary densities in ischemic legs increase gradually over 14 days (Figure 2D). It is very interesting, therefore, that the peak of VEGFR expression occurred ~ 9 days after the procedure. Furthermore, these data suggest that only a several-fold increase in the expression level of VEGFR on endothelial cells is critical for angiogenesis in ischemic tissues.

During angiogenesis, tip cells, stalk cells, and phalanx cells control vessel sprouting. Tip cells are located at the forefront of the sprouting vessel, stalk cells are located behind the tip cell at the branch, and phalanx cells are found in the unbranched endothelial layer.[13] Previous ex vivo studies reported that VEGFR expression in the tip cell is high to sense the VEGF concentration gradient in the extravascular area. In stalk cells, which control elongation of a new branch, VEGFR levels are lower than in the tip cells.[14] In phalanx cells, which normalize the endothelial cell layer, VEGFR levels are lower than in the stalk cells.[13] However, these are